# Simulations of Particle-Fluid Suspensions with the Lattice-Boltzmann Equation

Anthony J.C. Ladd
*Chemical Engineering Department*
*University of Florida, Gainesville, FL 32611-6005*

## 1. Introduction

The lattice-Boltzmann model [1,2] has become a popular method for modeling fluid-dynamical behavior, because of its robustness and simplicity. In essence, we follow the time evolution of a discrete velocity distribution, which describes the number of particles moving in a given direction at a given space and time point. Because the model lives on a regular lattice, the update of the population densities is very simple and very fast. The hydrodynamic fields are determined from moments of the velocity distribution function, as in the kinetic theory of gases. Somewhat surprisingly, studies show that this method can be as accurate as advanced finite-difference and finite-element methods [3-5], and it is usually more efficient for complicated geometries. Additionally, the lattice-Boltzmann model can incorporate thermal noise, leading to Brownian motion via random stresses applied to the fluid [6,7] rather than from random forces applied to the particles. This approach avoids the complex and time-consuming factorization of the mobility matrix that is necessary in every step of a Brownian dynamics simulation. In this short paper I will briefly summarize some recent applications of the method. Technical details can be found in Refs. [8-11].

## 2. Example Calculations

In this section I will describe simulations on a wide range of length scales, to illustrate the range of possibilities with this approach. At the largest scale we examine settling clusters of macroscopic particles under conditions where the Reynolds number is small, but not negligible. In the next example we investigate a chemically reacting flow in a porous medium, where the pore size is sufficiently small that inertia can be neglected. In the final example we show that the

method can reproduce theoretical scaling laws for the diffusion coefficient of long-chain polymers driven by thermal fluctuations in the fluid.

*2.1. Cluster Settling*

One of the most fascinating aspects of inertial particulate flows is their ability to make coherent patterns. These are stable and reproducible arrangements of particles that can spontaneously develop when fluid inertia is present. The best understood example of this phenomena is the inertial migration of particles in a pipe flow [12-15]. Equally interesting, but much less studied is the settling of a cluster of particles. In the absence of inertia, an initially spherical cluster maintains its shape as it settles, shedding a small trail of escaping particles in its wake [16]. At slightly higher Reynolds numbers, the cluster opens out fairly rapidly into a torus, which enlarges and thins as it settles [17]. Figure 1 shows the development of an initially spherical cluster of approximately 1800 particles, settling at a Reynolds number, $\mathrm{Re} = r\bar{U}d/m = 0.3$; here $r$ is the average fluid density, $\bar{U}$ is the mean particle velocity, $d$ is the particle diameter, and $m$ is the fluid viscosity.

The initially spherical cluster flattens into a pancake as particles peel off the leading edge of the cluster. Eventually a void develops in the core of the cluster and it assumes a toroidal shape. This is a highly coherent state, and no particles are lost from it. This is in contrast to what happens at low Reynolds number, when the cluster maintains an initially spherical shape indefinitely [16]. Eventually the ring becomes unstable and folds forward before breaking up into smaller clusters. The folding is characteristic of experimental observations as well [17], but in laboratory experiments the cluster usually, but not invariably, breaks up into two pieces rather than four as found here. We suspect that the periodic boundaries exert an influence on the shape of the cluster at long times, when it spans nearly the whole width of the simulated cell.

In terms of the fluid volume, this simulation was the largest we have so far attempted; 160 million grid points for 100,000 time steps. It required approximately 26 GBytes of memory and $5x10^{15}$ floating-point operations. The simulation took about 150 hours, distributed across 16 processors (2.4 GHz Xeons), using a one-dimensional domain decomposition. The aggregate performance was 32 million grid point updates per second, or about 20 GFlops. A video clip of the numerical simulations can be found at http://ladd.che.ufl.edu/research/clusters.

*2.2. Dissolution of a Rough Fracture*

The dissolution of a fractured rock by a reactive fluid depends on a subtle interplay between chemical reactions at mineral surfaces and fluid motion in the pores. The complex geometry of a typical fracture makes a first-principles calculation very demanding, and models of fracture dissolution are rarely constructed on a microscopic (pore-scale) level (but see [18-20]). The simulations describe the erosion of a synthetic fracture and incorporate the explicit topography of the pore space; the transport coefficients-viscosity, diffusivity, and reaction rate-are determined independently, so there are no fitting parameters.

The numerical simulations consist of a sequence of three separate calculations. First the fluid flow field in the pore space is calculated, using the exact topography of the solid surface. Given the flow field and the chemical kinetics at the solid surfaces, we determine the solute concentration field and then the local rate of dissolution over the whole fracture surface. Finally the fracture surfaces are eroded in proportion to the local dissolution rate and the whole process is repeated. The key assumption here is that the relaxation times of the velocity and concentration fields are much shorter than the characteristic relaxation time for dissolution. Within this quasi-static approximation, the velocity and concentration fields in the fracture reach a steady state for each configuration.

The velocity field in the fracture has been calculated using the lattice-Boltzmann method with "continuous bounce-back" rules applied at the solid-fluid boundaries [21]. These rules allow the solid surface to be resolved on length scales less than a grid spacing, so that the fracture surfaces erode smoothly. It has been shown that the flow fields in rough fractures can be calculated with one-half to one-quarter the linear resolution of the standard "bounce-back" rules [19], leading to an order of magnitude reduction in memory and computation time. A further order of magnitude saving in computation time can be obtained by solving for the steady-state directly by conjugate gradients [22], rather than by time stepping. These improvements have allowed us to calculate velocity fields in fractures with a characteristic size of several centimeters. For example, the calculation of a single flow field in the fracture illustrated in Fig. 2 takes 1 hour at the beginning and about 8 hours at the final stages of the dissolution process. The corresponding times for the conventional lattice-Boltzmann method would be measured in weeks rather than hours.

The numerical simulation algorithm was applied to the dissolution of a rough fracture of known topography, for which experimental dissolution patterns were available [23]. Solute transport in the fracture was modeled by a random walk algorithm that takes explicit account of the chemical reactions at the pore surfaces. At high Peclet numbers (high flow velocity) the under-saturated fluid penetrates deep inside the fracture and the dissolution tends to be uniform throughout the sample, but at lower flower rates the erosion is slower and much more inhomogeneous, with a clearly visible dissolution front. This front becomes unstable with respect to fingering instabilities [24], since an increase in permeability within a channel enhances solute transport, leading to faster growth of the channel. As the dissolution proceeds, the channels compete for flow and the growth of the shorter channels eventually ceases. At the end of the experiment, the flow is focused in a few main channels while most of the pore space is bypassed.

Sample dissolution patterns obtained by simulation and experiment are shown in Fig. 2 at a Peclet number Pe = 54. Here we define the Peclet number $\mathrm{Pe} = \bar{U}h_0/D$ in terms of the mean flow

velocity, $\bar{U}$, the initial value of the mean fracture aperture, $h_0$, and the molecular diffusion coefficient, *D*. The experimental and numerical dissolution patterns are strikingly similar [20]. The dominant channels develop at the same locations in the simulation and experiment, despite the strongly nonlinear nature of the dissolution front instability. While there are differences in the length of the channels, relatively small changes (of the order of 10%) in the diffusion constant or reaction rate can lead to comparable differences in the erosion patterns. Our results suggest that the simulations are capturing the effects of the complex topography of the pore space quite faithfully, despite the coarse aperture resolution of the flow solver.

*2.3. Hydrodynamic Interactions in Polymer Solutions*

Hydrodynamic interactions are a key component of simulations of polymer solutions; the diffusion coefficient of a linear polymer in good solvent scales as $N^{-0.59}$ with hydrodynamic interactions, where *N* is the number of segments, but as $N^{-1}$ in the free-draining limit. The motion of the individual monomers causes flow in the surrounding solvent, and the hydrodynamic interactions between distant segments of the chain have important consequences for the dynamics of polymer solutions. We have recently adapted the lattice-Boltzmann model to simulations of solutions of flexible polymers [25], by including the effects of thermal fluctuations via additional random stresses [8-10]. Since the individual segments are small in comparison to the size of polymer, we treat them as point sources hydrodynamically [26-28]. The diffusivity of an isolated polymer, shown in Fig. 3 as a function of chain length, is in quantitative agreement with the renormalization group analysis of the self-avoiding random walk [29]. The results are similar to Brownian dynamics [25], but at greatly reduced computational cost for large numbers of segments. While the maximum chain length that can be studied using Brownian dynamics is of the order of 100 beads [30,31], we have simulated chains with upwards of 1000 beads per polymer (Fig. 3).

## Conclusions

In this brief survey I have attempted to indicate the possible scope of simulations that are currently feasible within the framework of a lattice-Boltzmann model of the fluid. While we have found the method to be robust, reasonably accurate, and computationally efficient, it is important to emphasize that there is no new physics here. All these calculations can, at least in principle, be carried out within the framework of standard finite-difference or finite-element methods.

## References


1. McNamara, G.R. and G. Zanetti, Use of the Boltzmann equation to simulate lattice-gas automata. Phys. Rev. Lett., 1988; **61**: 2332.
2. Higuera, F., S. Succi, and R. Benzi, Lattice gas dynamics with enhanced collisions. Europhys. Lett., 1989; **9**: 345.
3. Breuer, M., et al., Accurate computations of the laminar flow past a square cylinder based on two different methods: lattice-Boltzmann and finite-volume. Int. J. Heat and Fluid Flow, 2000; **21**(2): 186-196.
4. Krafczyk, M., J. Tolke, and L.S. Luo, Large-eddy simulations with a multiple-relaxation-time LBE model. Int. J. Mod. Phys. B, 2003; **17**(1-2): 33-39.
5. Yu, H., S.S. Girimaji, and L.-S. Luo, Lattice Boltzmann simulations of decaying isotropic turbulence with and without system rotation. Phys Rev E (submitted), 2003.
6. Landau, L.D. and E.M. Lifshitz, Fluid Mechanics. 1959.
7. Ladd, A.J.C., Short-time motion of colloidal particles: Numerical simulation via a fluctuating lattice-Boltzmann equation. Phys. Rev. Lett., 1993; **70**: 1339.

8. Ladd, A.J.C., Numerical simulations of particulate suspensions via a discretized Boltzmann equation Part II. Numerical results. J. Fluid Mech., 1994; **271**: 311.

9. Ladd, A.J.C., Numerical simulations of particulate suspensions via a discretized Boltzmann equation Part I. Theoretical foundation. J. Fluid Mech., 1994; **271**: 285.

10. Ladd, A.J.C. Lattice-Boltzmann simulations of hydrodynamically interacting particles. in Dynamics: Models and Kinetic Methods for Non-equilibrium Many Body Systems. 2000: Kluwer Academic Publishers.

11. Nguyen, N.-Q. and A.J.C. Ladd, Lubrication corrections for in lattice-Boltzmann simulations of particle suspensions. Phys. Rev. E, 2002; **66**: 046708.

12. Ho, B.P. and L.G. Leal, Migration of rigid spheres in a 2-dimensional unidirectional flows. J. Fluid Mech., 1974; **65**: 365-400.

13. Asmolov, E.S., The inertial lift on a spherical particle in a plane Poiseuille flow at large channel Reynolds number. J. Fluid Mech., 1999; **381**: 63-87.

14. Schonberg, J.A. and E.J. Hinch, Inertial migration of a sphere in Poiseuille flow. J. Fluid Mech., 1989; **203**: 517-524.

15. Vasseur, P. and R.G. Cox, Lateral migration of a spherical particle in 2-dimensional shear flows. J. Fluid Mech., 1976; **78**: 385-413.

16. Nitsche, J.M. and G.K. Batchelor, Break-up of a falling drop containing dispersed particles. J. Fluid Mech., 1997; **340**: 161-175.

17. Nicolas, M., Experimental study of gravity-driven dense suspension jets. Phys. Fluids, 2002; **14**: 3570-3576.

18. Bekri, S., J.-F. Thovert, and P.M. Adler, Dissolution and Deposition in Fractures. Eng. Geol., 1997; **48**: 283-308.

19. Verberg, R. and A.J.C. Ladd, Simulations of Erosion in Narrow Fractures. Phys. Rev. E, 2002; **65**: 016701.

20. Szymczak, P. and A.J.C. Ladd, Microscopic simulations of fracture dissolution. Geophys. Res. Lett (In Press), 2004.

21. Verberg, R. and A.J.C. Ladd, Lattice-Boltzmann Model with Sub-Grid Scale Boundary Conditions. Phys. Rev. Lett., 2000; **84**: 2148-2151.

22. Verberg, R. and A.J.C. Ladd, Simulation of Low-Reynolds-Number Flow via a Time-Independent Lattice-Boltzmann Method. Phys. Rev. E, 1999; **60**: 3366-3373.

23. Detwiler, R.L., R.J. Glass, and W.L. Bourcier, Experimental observations of fracture dissolution: The role of Peclet number in evolving aperture variability. Geophys. Res. Lett., 2003; **30**: 1648.

24. Ortoleva, P., et al., Geochemical self-organisation I: The reactive-infiltration instability. Am. J. Sc., 1987; **287**: 1008-1040.

25. Usta, O.B., A.J.C. Ladd, and J.E. Butler, Lattice-Boltzmann simulations of the dynamics of polymer solutions in periodic and confined geometries. J. Chem. Phys. (Submitted), 2004.

26. Ahlrichs, P., R. Everaers, and B. Dunweg, Screening of hydrodynamic interactions in semidilute polymer solutions: A computer simulation study. Phys. Rev. E, 2001; **64**: 040501.

27. Ahlrichs, P. and B. Dunweg, Lattice-Boltzmann simulation of polymer-solvent systems. Int. J. Mod. Phys. C, 1998; **9**(8): 1429-1438.

28. Ahlrichs, P. and B. Dunweg, Simulation of a single polymer chain in solution by combining lattice Boltzmann and molecular dynamics. J. Chem. Phys., 1999; **111**(17): 8225-8239.

29. Oono, Y. and M. Kohmoto, Renormalization group theory of transport properties of polymer solutions. I. Dilute solutions. J. Chem. Phys., 1983; **78**: 520-528.

30. Jendrejack, R.M., et al., Shear-induced migration in flowing polymer solutions: Simulation of long-chain DNA in microchannels. J. Chem. Phys., 2004; **120**: 2513-2529.

31. Hsieh, C.-C. and R.G. Larson, Modeling hydrodynamic interaction in Brownian dynamics: Simulations of extensional and shear flows of dilute solutions of high molecular weight polystyrene. J. Rheol., 2004; **48**: 937-1184.

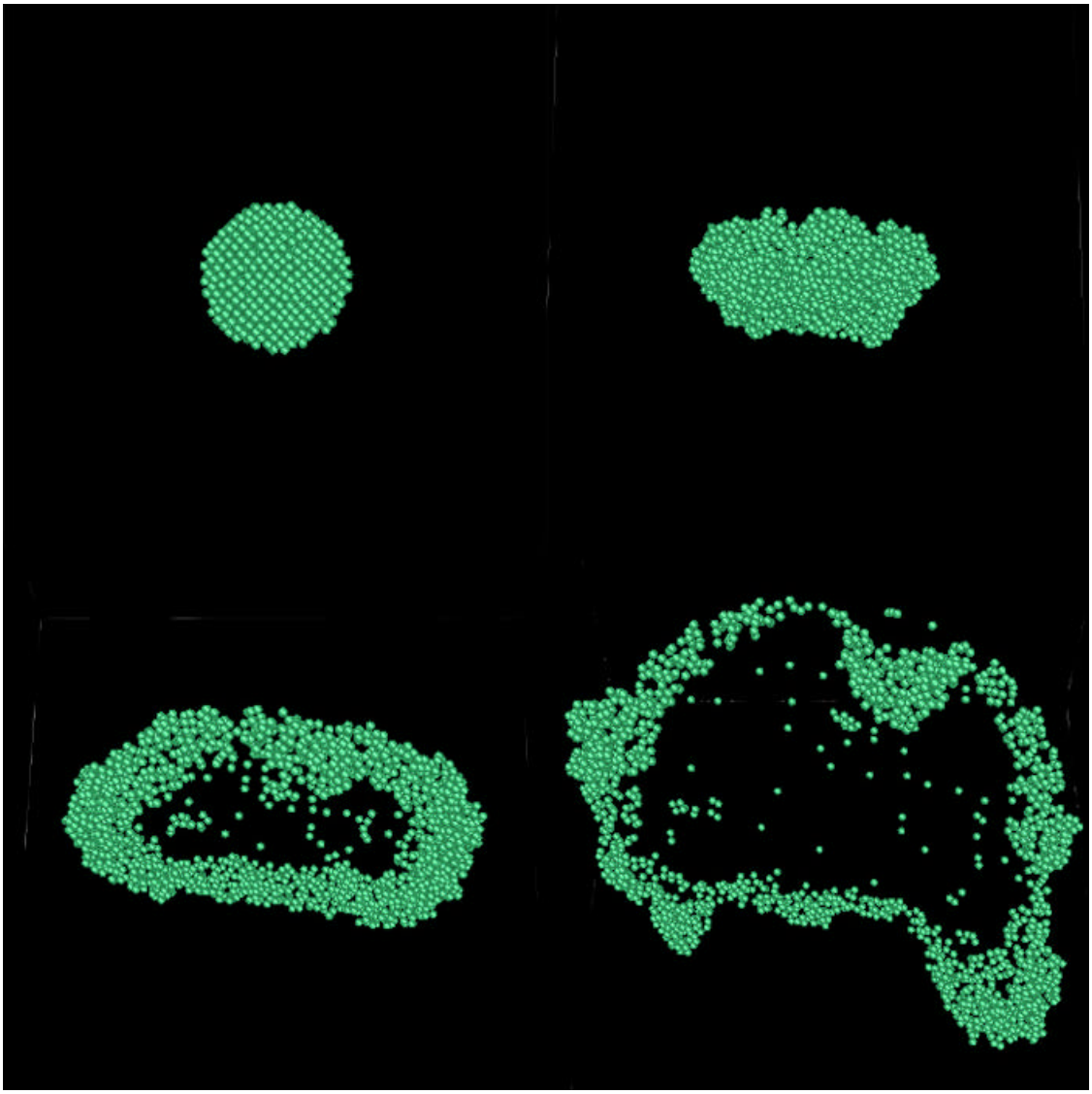

Figure 1. Evolution of a spherical cluster of particles (~1800) settling under gravity. The initially spherical cluster (top left) flattens into a pancake shape (top right) and develops into a stable torus (bottom left). Eventually the torus thins and breaks up (bottom right) into smaller clusters, which also assume a toroidal shape and break up in the same way.

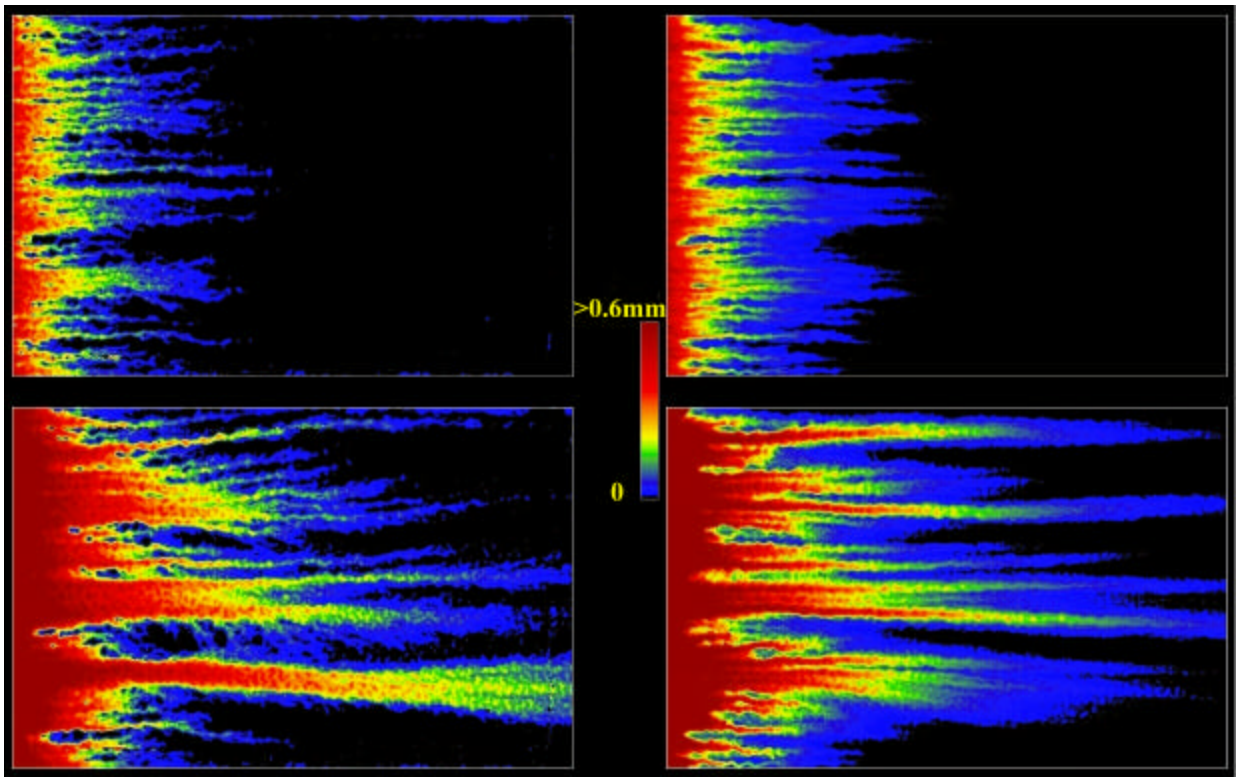


Figure 2 Aperture growth due to dissolution of a KDP fracture at Pe = 54. The figures show dissolution patterns at $\Delta h = h_0/2$ (upper) and $\Delta h = h_0$ (lower). The experimental results are shown on the left and the corresponding simulation results are on the right. The flow direction is from left to right.

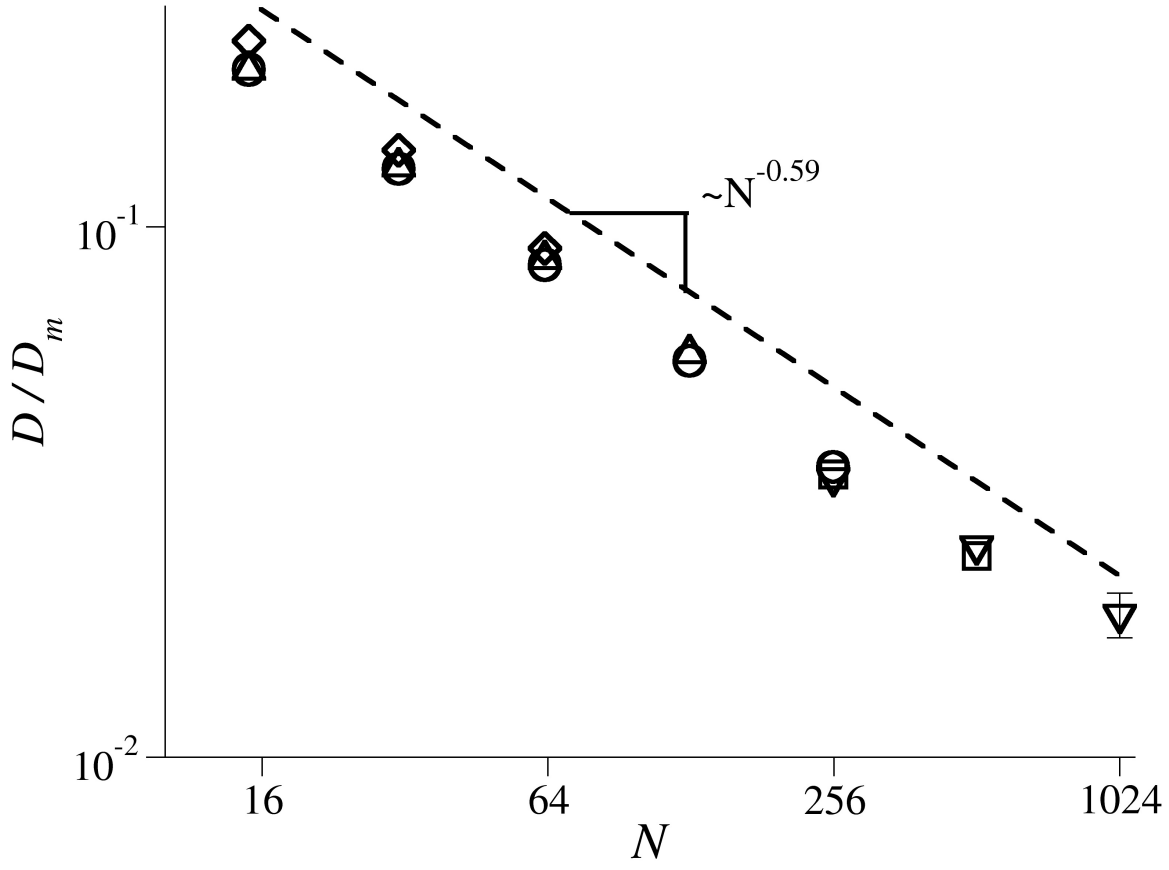


Figure 3. Diffusion coefficient of an $N$-bead polymer, $D$, compared with the monomer diffusivity, $D_m$. Results are shown for different segment lengths and different temperatures. The slope of $-0.59$ agrees closely with the theoretical prediction.